

Assembly of endocytic machinery around individual influenza viruses during viral entry

Michael J Rust^{1,2}, Melike Lakadamyali^{1,2}, Feng Zhang¹ & Xiaowei Zhuang¹

Most viruses enter cells via receptor-mediated endocytosis. However, the entry mechanisms used by many of them remain unclear. Also largely unknown is the way in which viruses are targeted to cellular endocytic machinery. We have studied the entry mechanisms of influenza viruses by tracking the interaction of single viruses with cellular endocytic structures in real time using fluorescence microscopy. Our results show that influenza can exploit clathrin-mediated and clathrin- and caveolin-independent endocytic pathways in parallel, both pathways leading to viral fusion with similar efficiency. Remarkably, viruses taking the clathrin-mediated pathway enter cells via the *de novo* formation of clathrin-coated pits (CCPs) at viral-binding sites. CCP formation at these sites is much faster than elsewhere on the cell surface, suggesting a virus-induced CCP formation mechanism that may be commonly exploited by many other types of viruses.

Many viruses infect their host cells through endocytosis. The endocytic pathways used by some viruses have been determined, but the entry mechanisms for most remain poorly understood^{1–9}. This is in part because of the presence of several endocytic pathways that may be exploited by viruses, including both clathrin- and caveolin-mediated endocytosis, as well as clathrin- and caveolin-independent pathways^{10–14}. Another important question in viral entry is the way in which viruses are targeted to endocytic machinery for internalization. This is a critical and largely open question for other endocytic ligands as well¹¹. For clathrin-mediated endocytosis, ligands and bound receptors are targeted to CCPs; then the CCPs mature into clathrin coated vesicles (CCVs), resulting in the internalization of ligands and receptors. Two different targeting mechanisms are possible: (i) ligands and bound receptors may be targeted to pre-existing CCPs on the cell surface, and (ii) clathrin and cofactors may be recruited to the site of the bound ligand, leading to *de novo* formation of a CCP at that site. So far, only the first mechanism has been directly observed^{15,16} by detecting single CCPs in living cells¹⁷. A direct observation of the second scenario may be more challenging, because it requires the real-time detection of single ligand molecules or particles simultaneously with single CCPs.

Because of its medical importance, influenza has long been used as a model system to understand viral entry mechanisms. Influenza viruses enter cells through receptor-mediated endocytosis and then progress to late endosomes, where viral fusion leads to the release of the viral genome^{1,9,18–23}. Although it has been established that influenza viruses bind to the terminal sialic acid of glycoproteins and glycolipids on the cell surface¹⁸, little is known about how these viruses are targeted to cellular endocytic structures after binding.

The exact endocytic pathway exploited by influenza is also unclear. Electron microscopy of virus-infected cells has revealed influenza

viruses inside CCPs and CCVs as well as inside smooth pits and vesicles¹, whereas Semliki Forest viruses have only been found to associate with coated structures²⁴. However, without real-time imaging, it is unclear whether these smooth pits lead to influenza entry, nor is it known whether the smooth virus-bearing vesicles result from uncoating of CCVs or from clathrin-independent endocytosis. A recent study shows that dominant-negative mutants and drugs that specifically block clathrin- and caveolin-mediated endocytosis do not substantially affect the infectivity of influenza⁸. This indicates that the virus can infect cells through a clathrin- and caveolin-independent pathway(s), although it is unclear whether this pathway is used by influenza viruses under unperturbed cellular conditions. The relative significance of the clathrin-mediated and clathrin- and caveolin-independent pathways in influenza viral infection is at present unknown. The molecular mechanism of the clathrin- and caveolin-independent pathway also remains largely elusive.

In this study, we used real-time fluorescence microscopy to simultaneously track individual influenza viruses and endocytic structures in living cells. This allowed us to characterize the endocytic mechanism exploited by each virus without inhibiting specific endocytic pathways. In addition, the ability to monitor individual viruses in real time provides previously unavailable information about the dynamics of endocytic processes and is particularly well suited to address how viruses are targeted to endocytic machinery. Our single-virus studies show that influenza viruses enter cells via multiple endocytic pathways, with both the clathrin-mediated pathway and a clathrin- and caveolin-independent pathway(s) significantly populated. Both pathways lead to viral fusion with intracellular membrane compartments and thus, presumably, to the release of the viral genome. Simultaneous tracking of single viruses and single CCPs shows that viruses

¹Department of Chemistry and Chemical Biology, Harvard University, 12 Oxford Street, Cambridge, Massachusetts 02138, USA. ²These authors contributed equally to this work. Correspondence should be addressed to X.Z. (zhuang@chemistry.harvard.edu).

Published online 2 May 2004; doi:10.1038/nsmb769

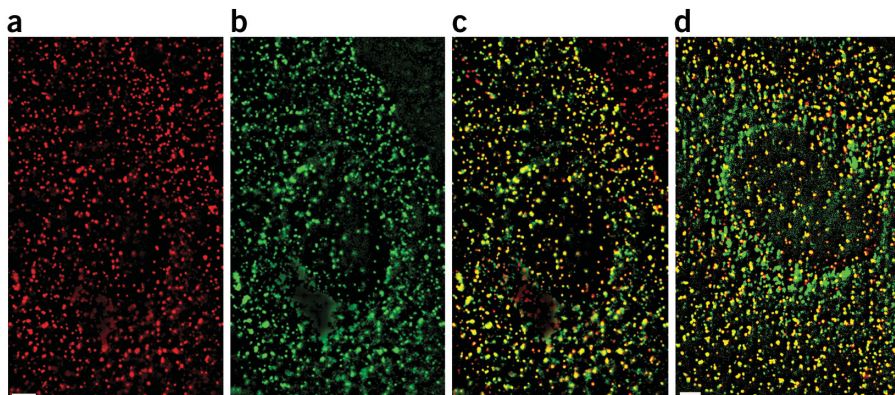


Figure 1 Fluorescence images of clathrin-coated structures in BS-C-1 cells expressing EYFP-clathrin. For a clearer visualization of discrete fluorescent spots, a low-spatial frequency background due to cytoplasmic EYFP-clathrin has been subtracted from the images. Scale bars, 3 μ m. (a) Immunofluorescence image of clathrin-coated structures in a cell transiently transfected with EYFP-clathrin. (b) EYFP fluorescence image of clathrin-coated structures in the same cell. (c) Overlay of the immunofluorescence signal (red) with the EYFP signal (green). Pixels with both red and green signal appear yellow. Counting spots in several cells shows that >97% of the clathrin-coated structures that appeared in the immunofluorescence image colocalized with those in the EYFP image. The red-only spots in the upper right corner of the image belong to a neighboring cell not transfected with EYFP-clathrin. (d) Overlay of the transferrin image (red) and EYFP image (green) of a cell stably expressing EYFP-clathrin. Alexa Fluor 647-labeled transferrin (Molecular Probes) was bound to cells at 4 °C for 15 min. After removing unbound transferrin, cells were imaged at room temperature. An image averaged over the first 5 s is shown. Over 96% of the transferrin spots colocalize with clathrin-coated structures and appear yellow.

exploiting the clathrin-mediated pathway are internalized through the *de novo* formation of CCPs around the viruses. We have resolved the formation and disassembly dynamics of these CCPs and CCVs in real time. Notably, the CCP formation rate is much higher at the sites of bound viruses than elsewhere on the cell surface. The kinetics of CCP formation at these sites suggests that the formation is most probably induced by viral binding.

RESULTS

Imaging endocytic structures and viruses

To visualize endocytic structures in cells, we expressed clathrin or caveolin fused to fluorescent proteins following previously established procedures^{7,17,25,26}. Briefly, we constructed a plasmid encoding enhanced yellow fluorescent protein (EYFP) attached to clathrin light chain *a* (LCa). This fusion protein was expressed in BS-C-1 cells. The functional integrity of clathrin is not compromised by fluorescent protein labels^{17,25,27,28}. The distribution of EYFP-labeled clathrin (EYFP-clathrin) in cells shows discrete, dynamic fluorescent structures (Fig. 1 and Supplementary Video 1 online). To test whether the EYFP image reveals all CCPs and CCVs, we immunolabeled these structures with an antibody against the AP2 complex, an abundant protein in CCPs and CCVs. Over 97% of discrete structures in the immunofluorescence image colocalize with those in the EYFP image (Fig. 1c)^{17,25}. In addition, we imaged fluorescently labeled transferrin, a known marker for clathrin-mediated endocytosis, and found that >96% of transferrin spots colocalize with EYFP-clathrin structures before their internalization (Fig. 1d). These spots were subsequently internalized as indicated by microtubule-dependent movement and disappearance of the associated EYFP-clathrin signal (data not shown). These observations suggest that our EYFP fluorescence images reveal nearly all CCPs and CCVs in living cells.

Similarly, we expressed enhanced green fluorescent protein (EGFP)-tagged caveolin-1 (caveolin-1-EGFP) in BS-C-1 cells^{7,26,29,30}. The distribution of caveolin-1-EGFP in cells shows discrete fluorescent structures (Supplementary Video 2 online), which were previously suggested to be individual caveolae and caveosomes^{7,26,29,30}. Nearly perfect colocalization has been found between the caveolin structures in the EGFP image and those in the immunofluorescence image obtained using antibodies against caveolin (data not shown)⁷. The cholera toxin subunit β , a known marker for caveolin-mediated endocytosis³¹, was successfully internalized via labeled caveolae in these cells expressing caveolin-1-EGFP (Supplementary Fig. 1 online), indicating that the EGFP label did not markedly perturb the internalization of caveolae⁷.

To visualize individual viruses in living cells^{32–36}, we labeled the influenza virus with a lipophilic dye, DiD. This labeling does not affect viral infectivity³⁶. Tracking of single viruses revealed a three-stage active transport process (Fig. 2) similar to what we have observed previously in CHO cells, with stage I being an actin-dependent movement on the cell surface and/or in the cell periphery, stage

II being a rapid, unidirectional movement on the microtubule toward the perinuclear region and stage III being a bidirectional, microtubule-dependent movement³⁶. The dependence of these movements on actin or microtubules was tested with actin- or microtubule-disrupting drugs using similar methods to those of our previous study³⁶. Here we used the onset of the microtubule-dependent stage II movement to indicate that internalization of the virus has already occurred. We then determined the endocytic mechanism responsible by examining the colocalization of the virus with CCPs and caveolae before this movement.

Multiple influenza entry pathways

To determine whether influenza viruses are internalized through clathrin-mediated endocytosis, we infected BS-C-1 cells expressing EYFP-clathrin with DiD-labeled viruses and imaged individual viruses and clathrin-coated structures simultaneously (Supplementary Video 1 online). We found that most viruses had been internalized into the cells as indicated by the microtubule-dependent stage II movement. The average time between viral binding and stage II movement is ~5.6 min, in quantitative agreement with that obtained in cells not expressing EYFP-clathrin³⁶. About 65% of the internalized viruses had associated with a discrete clathrin-coated structure for an extended period of time, followed by a rapid disappearance of the clathrin signal (Fig. 2a,b and Supplementary Videos 3 and 4 online), suggesting the internalization of the viruses via CCPs and the rapid uncoating of CCVs afterwards. The remaining 35% of the viruses did not show any association with clathrin-coated structures before stage II movement (Fig. 2c and Supplementary Video 5 online), suggesting their internalization via a clathrin-independent pathway. Similar partition values were obtained for experiments conducted at various times (≥ 24 h) after transfection with EYFP-clathrin and for

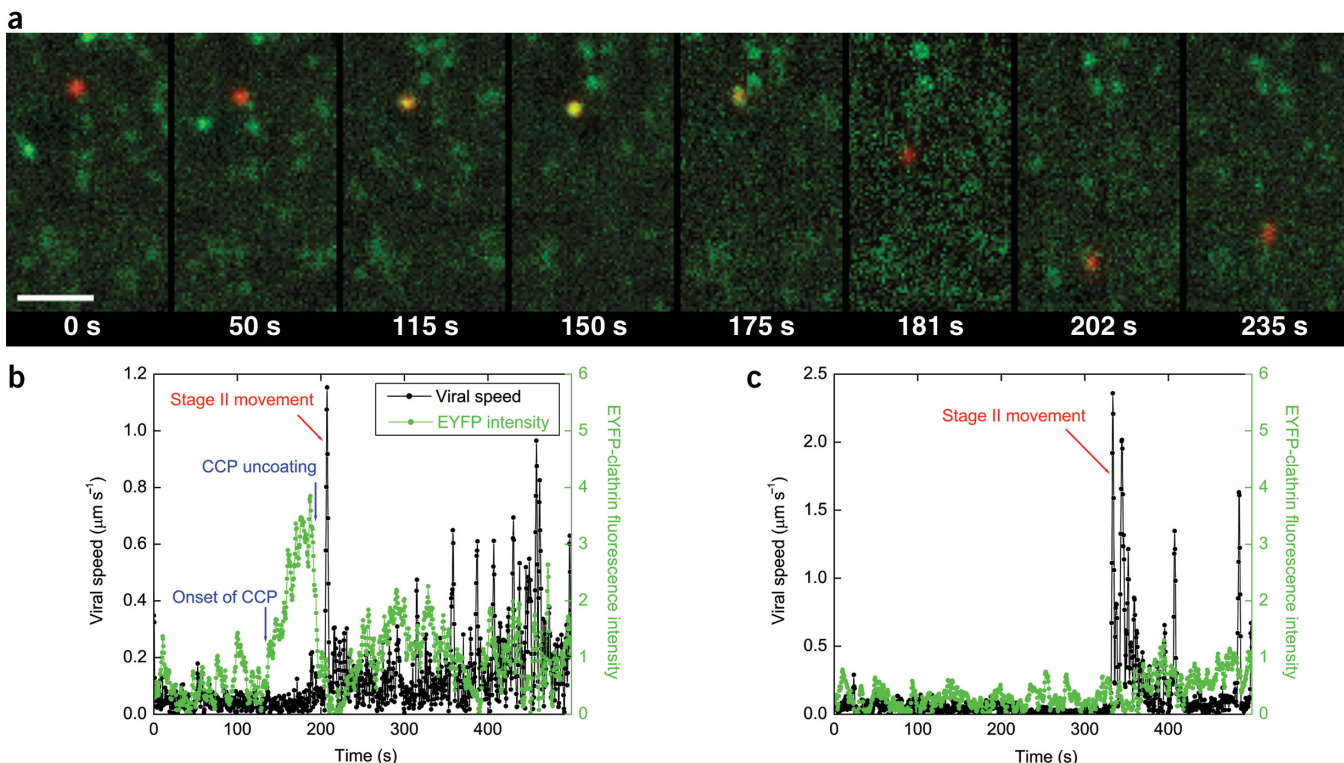


Figure 2 Internalization of influenza viruses through different pathways. (a) Snapshots of a virus internalized through a CCP. A live movie of this virus is available as **Supplementary Video 3** online. Scale bar, 10 μ m. At $t = 0$ s, the virus (red) binds to the cell. At $t = 50$ s, the virus is undergoing stage I movement. At $t = 115$ s, a CCP labeled with EYFP (green) begins to form at the virus site. At $t = 150$ s, the clathrin coat reaches its peak fluorescence intensity. At $t = 175$ s, the clathrin coat rapidly disassembles. At $t = 181$ s, the virus is transported toward the perinuclear region on a microtubule (stage II movement). At $t = 202$ s, the virus enters stage III transport involving both plus- and minus-end-directed motilities on microtubules. At $t = 235$ s, the virus continues stage III movement. (b) The time trajectories of a virus internalized through *de novo* formation of a CCP. Black symbols, velocity-time trajectories of the virus. Stage II movement is identified as the rapid unidirectional translocation from the cell periphery to the perinuclear region (red arrows). Green symbols, integrated fluorescence intensity of EYFP-clathrin associated with the virus. (c) The time trajectories of a virus internalized without association with a clathrin-coated structure. Symbols are as defined in b. Live movies of the two viruses in b and c are also available (**Supplementary Videos 4** and **5** online).

infection in cells stably expressing EYFP-clathrin. This partition was also independent of the excitation laser intensity used. The same partition ratio was obtained when we used the initial acidification of virus particles to pH 6 (ref. 36), instead of stage II movement, as an indication that they had already been internalized into intracellular endocytic compartments (data not shown).

De novo formation of CCPs around viruses

Tracking the behavior of individual viruses also allowed us to determine how viruses internalized through the clathrin-mediated pathway were targeted to CCPs. Our quantitative analysis shows that only 6% of the viruses joined with a pre-existing CCP. The remaining 94% were internalized through the *de novo* formation of a CCP at the virus-binding sites: these viruses initially bound to sites that showed no discrete EYFP-clathrin signal, and then a fluorescent EYFP spot appeared that was centered on the virus, typically 2–3 min after viral binding. The EYFP fluorescence intensity gradually increased and then rapidly disappeared before the virus started stage II movement (Fig. 2a,b and **Supplementary Videos 3** and **4** online). Our quantitative analysis of the relative displacement between the CCP and the virus confirms the visual impression that CCP formation begins directly centered on the virus (**Supplementary Fig. 2** online). We occasionally observed clathrin structures passing by, temporarily colocalizing with and then separating from viruses. These events are not counted as clathrin-mediated endocytosis.

Dynamics of clathrin-mediated endocytosis

Real-time observation of the entire formation and disassembly process of CCPs and CCVs around the viruses allowed us to determine the dynamics of the process (Fig. 3). The formation of CCPs is initiated on average 190 s after the viruses bind to the cell (Fig. 3a). The probability of CCP formation increases with time initially and peaks after a lag of 170 s following viral binding (Fig. 3a). The clathrin signal persists for ~70 s on average (Fig. 3b). This period includes a clathrin accumulation phase with a roughly linearly increasing clathrin intensity that indicates the recruitment of clathrin to form a CCP, which then pinches off from the plasma membrane to form a CCV, followed by rapid uncoating of the CCV that is typically completed in only a few seconds (Fig. 3b). The lifetimes of the virus-bound CCPs are similar to those of the constitutive CCPs not associated with viruses (data not shown).

The above results show that the viruses were not typically targeted to pre-existing CCPs but were predominantly internalized via CCPs that formed *de novo* at the site of the bound viruses. However, this does not necessarily imply that the formation of these pits is induced by viral binding. As CCPs are constitutively forming on the cell surface, the possibility exists that a CCP would by chance form at the virus site. To address this possibility, we analyzed the formation rate of CCPs at random sites on the cell surface. Notably, we found that the formation rate at random sites was 20 times lower than that at the sites of bound viruses.

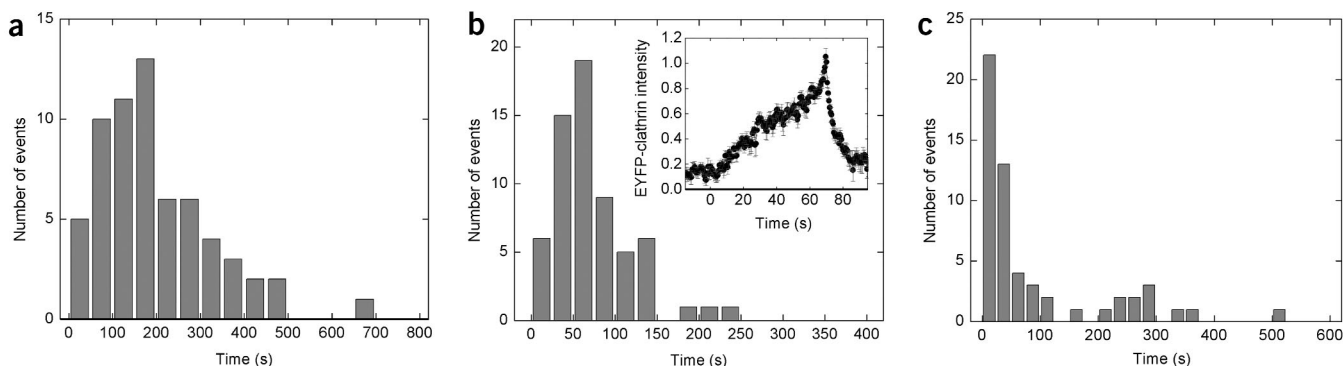


Figure 3 Dynamics of the CCPs and CCVs formed *de novo* at the virus-binding sites. **(a)** Histogram of the time between viral binding and onset of CCP formation. **(b)** Histogram of the time between the onset of CCP formation and CCV uncoating. Inset: an averaged curve of 60 time trajectories of the EYFP-clathrin intensity associated with viruses shows the life cycle of CCPs. Each EYFP-clathrin trajectory was normalized to the peak height and scaled in time so that the onset of the CCP formation occurs at $t = 0$ s and the peak clathrin intensity occurs at $t = 69$ s, which is the average duration of the clathrin accumulation phase. **(c)** A histogram of the time between the first CCV uncoating event and the onset of stage II viral movement.

Is it then possible that the viruses are captured by 'hot spots' on the cell surface that have a higher CCP formation rate^{17,25}? To look for these hot spots, we chose sites of pre-existing CCPs and analyzed the waiting time for another CCP to form at the same or nearby sites after the initial CCP had disappeared. The CCP formation rate obtained at these sites is, however, similar to the rate obtained at random sites on the cell surface. Only at <5% of the pre-existing-CCP sites did we observe a rapidly 'blinking' fluorescent spot that may indicate repetitive CCP formation^{17,25}. In addition, the 'dark' times at these blinking sites are only ~10–20 s, much shorter than the average time it takes for a CCP to appear at a virus-binding site both before and after the viral binding event. These results indicate that the *de novo* CCP formation at the virus-binding sites is not due to static hot spots on the cell surface.

The possibility remains that the observed high CCP formation rate is due to preferential association of viruses with mobile hot spots that have a higher CCP formation rate. If the viruses were indeed internalized by binding to these hypothetical hot spots and did not influence the CCP formation rate there, then the probability that a CCP appears at these sites should be independent of time relative to viral binding, and the distribution of the relative time (T_1) between viral binding and CCP formation should follow an exponential decay without any lag. This is inconsistent with our observed T_1 distribution, which shows a substantial lag (Fig. 3a). Could the lag be caused by the relative movement between viruses and hot spots on the cell surface before their association? If so, the average time it takes a CCP to appear at the hot spots should be less than $\langle T_1 \rangle$ (190 s). Considering that the average duration of a CCP is 70 s, the probability of finding a CCP at the hot spots should be >27% at any time. Thus, if viruses move to the hot spots to be internalized, the fraction of viruses that joined with a pre-existing CCP should be >27%, again inconsistent with our observed value (6%). These results suggest that the CCPs that appear *de novo* at the sites of the bound viruses are most probably induced or influenced by viral binding.

After clathrin uncoating, the viruses show heterogeneous transport dynamics. The majority of viruses started their microtubule-dependent movement <40 s after uncoating, whereas the rest remained in the cell periphery for several minutes before stage II movement (Fig. 3c and Supplementary Fig. 3 online). For the latter fraction of viruses, the relatively long lag between clathrin uncoating and stage II movement leaves open the possibility that the viruses were

recycled back to the cell surface and were then again endocytosed. Indeed, we occasionally observed a second round of CCP formation during that period. If the hypothetical re-endocytosis events occur through a clathrin-independent mechanism, it could lead to a moderate effect on the partition ratio of viruses between the clathrin-dependent and independent pathways, as we detail in Supplementary Figure 3 online.

Effect of neuraminidase on influenza entry

Influenza viruses bind to sialic acids on cell surfaces through hemagglutinin in a highly multivalent manner. Such multivalent binding could restrict viral mobility on the cell surface. Influenza neuraminidase cleaves bonds between hemagglutinin and the cell surface³⁷. It is thus possible that neuraminidase activity facilitates viral movement on the cell surface and targeting to endocytic sites and, therefore, functions importantly in cellular entry of influenza. However, our observation of *de novo* CCP formation at viral-binding sites suggests that neuraminidase activity may not be critical for the internalization of influenza. To test this, we investigated the cellular entry of influenza in the presence of neuraminidase inhibitors RWJ-270201 and oseltamivir^{38,39}. Whereas these inhibitors effectively block influenza infection at a concentration <100 nM (data not shown)^{38,39}, we failed to observe their effect on viral endocytosis, trafficking and fusion even at a concentration of 1 μ M. The relative time between viral binding and the stage II movement is very similar to that in the absence of drugs (Fig. 4), suggesting that neuraminidase is not essential for the cellular entry of influenza and that these recently developed influenza drugs function to block other stages of the infection³⁷.

The clathrin- and caveolin-independent pathway

Next, we addressed the internalization mechanism of viruses that entered cells without colocalization with CCPs. To this end, we infected BS-C-1 cells expressing caveolin-1-EGFP with DiD-labeled viruses and imaged individual viruses together with caveolae and caveosomes (Supplementary Video 2 online). We found that most viruses had been internalized into the cells, as indicated by the onset of stage II movement, and the average time between viral binding and stage II movement was similar to that in cells not expressing caveolin-1-EGFP. Among the internalized viruses, <5% showed colocalization with caveolae and caveosomes before internalization. In cells treated with filipin (5 μ g ml⁻¹), an inhibitor of caveolin-mediated endocytosis⁴⁰, we observed a similar partition ratio of viruses between the

clathrin-dependent and independent pathways to that in untreated cells, whereas the same filipin treatment blocks the internalization of cholera toxin subunit β (M.L., M.J.R. and X.Z., unpublished data). The above observations indicate that the clathrin-independent endocytic pathway exploited by influenza is also independent of caveolin and lipid rafts¹⁴.

To initiate infection, influenza viruses release their genome into the cytoplasm by fusing with endosomes^{1,9,18–23}. We tested whether the clathrin-mediated pathway and clathrin- and caveolin-independent pathway(s) both lead to viral fusion. To this end, we labeled the viruses with a high surface density of DiD such that its fluorescence is partially quenched. Viral fusion events can be identified by a marked increase in the DiD fluorescence intensity due to fusion-induced dequenching (Fig. 5 and Supplementary Videos 6 and 7 online)³⁶. Among the viruses that fused, 69% had shown association with clathrin-coated structures before stage II movement, whereas 31% had not. This partition is almost identical to that obtained for all viruses showing microtubule-dependent movement.

Next, we compared the trafficking kinetics of viruses along both clathrin-dependent and clathrin-independent pathways. The distributions of time between viral binding and stage II movement are similar for the two pathways (Supplementary Fig. 4a online). This would not be surprising if the two endocytic pathways were competing for viral entry. The time distributions between stage II movement and viral fusion are also similar for the two pathways (Supplementary Fig. 4b online). This may in part be caused by the convergence of clathrin-mediated and clathrin-independent pathways in endocytic trafficking⁴¹. We have indeed observed merging events of virus-containing vesicles internalized through the two pathways before viral fusion. These results are consistent with a previous finding that influenza viruses enter endosomes at similar times regardless of whether dominant-negative mutants are present to block clathrin-mediated endocytosis⁴². The distances between the fusion sites and the nuclear envelope are also similar for viruses entering through the two pathways (Supplementary Fig. 4c online).

The above results indicate that the clathrin-mediated and clathrin-independent pathways are equally efficient for viral fusion once the viruses are internalized. Considering previous observations that influenza viruses fuse with endosomes to release their genome and initiate infection^{1,9,18–23} and that influenza infects cells in the presence of drugs and mutants that block clathrin- and caveolin-mediated endocytosis⁸, our data suggest that the two pathways are probably equally efficient for infection once the viruses are internalized. Our results further show that clathrin- and caveolin-independent endocytosis is not an alternative means exploited by influenza only when clathrin-dependent endocytosis is blocked, but a parallel pathway that influenza takes under normal cellular conditions.

DISCUSSION

Although receptor-mediated endocytosis is known to be one of the major mechanisms that viruses exploit to enter cells, the molecular mechanisms underlying the complex processes of viral endocytosis are still poorly understood. In this work, we have visualized single influenza viruses and endocytic structures in living cells and tracked the interaction between them in real time using fluorescence microscopy. This has allowed us to determine the endocytic mechanisms exploited by influenza without inhibiting specific endocytic pathways and to address directly how influenza viruses are targeted to endocytic machinery for internalization.

Our single-virus trajectories show that influenza viruses enter cells through at least two endocytic pathways. In any given infection

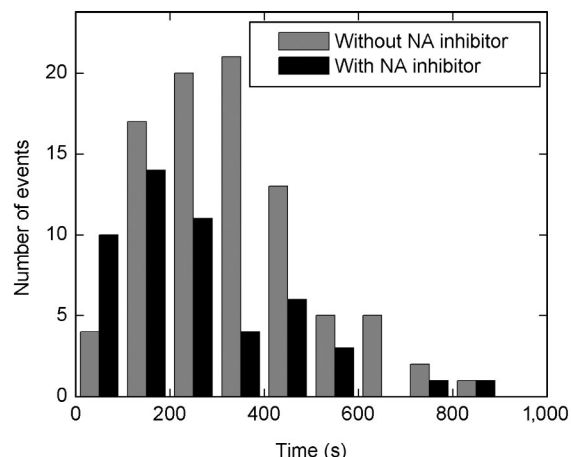


Figure 4 The effect of neuraminidase (NA) inhibitors on the endocytosis of influenza viruses. Gray columns, histogram of the time between viral binding and the onset of stage II movement in the absence of NA inhibitors. Black columns, histogram in the presence of 1 μ M RWJ-270201. The histogram in the presence of 1 μ M oseltamivir is similar (data not shown).

experiment, roughly two-thirds of the viruses enter cells through clathrin-mediated endocytosis and the remaining through a clathrin- and caveolin-independent endocytic pathway(s). Both pathways lead to viral fusion with intracellular membrane compartments with a similar efficiency.

By tracking the interaction between viruses and CCPs in real time, we show that the viruses exploiting the clathrin-mediated pathway are predominantly (94%) internalized through *de novo* formation of CCPs around the viruses. Although recruitment to pre-existing CCPs has been observed previously for G protein-coupled receptors^{15,16}, the *de novo* formation of CCPs at the sites of bound ligands has not been directly observed before. We have resolved the dynamics of CCP formation around the viruses: clathrin begins to appear at the viral-binding sites a few minutes after binding; this is followed by a roughly linear increase in clathrin intensity for \sim 1 min, during which time a CCP is formed and matures into a CCV. Immediately after the clathrin intensity reaches its maximum, the clathrin coat rapidly disassembles, typically in only a few seconds. Notably, we found that the formation rate of CCPs was 20 times higher at the sites of bound viruses than elsewhere. The formation kinetics of CCPs at these sites suggests that the formation is most probably induced by viral binding.

Ligand-induced clathrin redistribution to the plasma membrane has been reported for epidermal growth factor (EGF) and nerve growth factor (NGF)⁴³. There, the binding of EGF to its receptor causes phosphorylation of the clathrin heavy chain and a global redistribution of clathrin to the cell periphery to form CCPs⁴⁴. The majority of newly induced CCPs do not actually colocalize with the NGF receptors^{45,46}. This is distinct from our observations of *de novo* formation of CCPs at the virus-binding sites without a global redistribution of clathrin upon viral binding.

A question arises: considering that influenza viruses are believed to bind to sialic acids of glycolipids and glycoproteins on the cell surface instead of specific receptors with known internalization motifs, how is the signal of viral binding transmitted across the plasma membrane to initiate the recruitment of clathrin and associated factors and induce the formation of a CCP at the binding site? One possible mechanism stems from the highly multivalent binding of influenza to the cell through several bonds between hemagglutinin and sialic acid. This

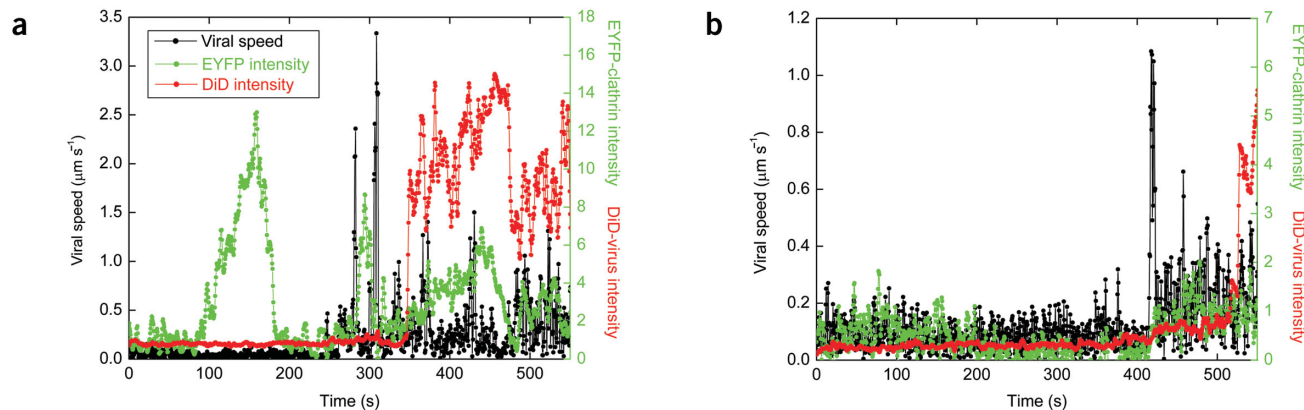


Figure 5 Time trajectories of viruses that successfully fused after endocytosis. **(a)** Example of a virus that was internalized through a CCP. **(b)** Example of a virus that was internalized without association with a CCP. Live movies of these two viruses are available (**Supplementary Videos 6** and **7** online). Viral fusion can be identified as a marked increase of the DiD signal.

highly multivalent binding of the virus to the cell surface may induce local curvature on the plasma membrane, thereby promoting formation of a CCP at the binding site. Notably, the most conserved domain (BAR domain) of amphiphysin, a component of CCPs, forms a crescent-shaped dimer that preferentially binds to highly curved negatively charged membranes⁴⁷. Whereas the wild-type amphiphysin can efficiently recruit clathrin to liposomes and polymerize clathrin into an invaginated lattice on a lipid monolayer, an amphiphysin with mutations in the BAR domain lacks such ability⁴⁷. We speculate that amphiphysin or other proteins with a similar BAR domain preferentially bind to the curved plasma membrane at the influenza virus-binding sites and promote CCP formation at those sites.

METHODS

Viruses and fluorescent labeling. Influenza virus X-31 was purchased from Charles River Laboratories. For labeling with lipophilic dyes, the viruses were incubated with DiD (Molecular Probes) for 2 h at 22 °C. Unbound dye was removed by buffer exchange into 50 mM HEPES, pH 7.4, 145 mM NaCl, using gel filtration columns. Immediately before experiments, viral aggregates were removed with 0.2-μm pore size filters.

Cell culture. BS-C-1 cells were maintained in a 5% CO₂ environment in MEM (Invitrogen) with 10% (v/v) FBS and passaged every 2–3 d. For fluorescence imaging, BS-C-1 cells were cultured in MEM with 10% (v/v) FBS in Petri dishes with glass coverslips on the bottom. Before fluorescence experiments, cells were washed in serum-free, phenol red-free medium fortified with 100 mM HEPES, pH 8.0.

Plasmids. We obtained the GFP-clathrin-LCa construct as a gift from J.H. Keen¹⁷. From this construct, the clathrin LCa cDNA was PCR-amplified to introduce an *Xba*I restriction site at the 5' end and an *Age*I restriction site at the 3' end. Similarly, we amplified the EYFP cDNA, introducing an *Xba*I restriction site at the 3' end. The EYFP PCR product was inserted into the pcDNA3.1/V5-His-TOPO vector (Invitrogen). This construct was then digested with *Age*I and *Xba*I (New England Biolabs), and the clathrin-LCa PCR product was ligated using these sites into the vector containing EYFP, yielding a cDNA coding for a chimeric protein with EYFP fused to the N terminus of clathrin-LCa. The caveolin-1-EGFP construct was a gift from A. Helenius⁷.

Transfection of cells. Cells were transfected with EYFP-clathrin-LCa or caveolin-1-EGFP using FuGENE 6 transfection reagent (Roche). For a 60-mm Petri dish to be transfected, 2 μl of FuGENE 6 reagent was combined with MEM and 1 μg of DNA for a final volume of 100 μl. The FuGENE-DNA mixture was incubated at room temperature for 20 min, added to the cell culture and then incubated in a 5% CO₂ environment.

Cells stably expressing EYFP-clathrin. The stable cell line was created using the RetroMax retroviral expression system (Imgenex). The EYFP-LCa gene was inserted into the *Hind*III-*Clal* restriction sites of the pCLNCX retrovirus expression vector (Imgenex) that confers G418 resistance. 293T cells, growing in DMEM containing 10% (v/v) FBS, were then transfected using this vector and the pCL-10A1 retrovirus packaging vector (Imgenex). 293T supernatant was collected after 2 d and filtered through 0.45-μm pore size filters. The target BS-C-1 cells were then infected with an equal volume mix of the 293T supernatant with cell medium (MEM containing 10% (v/v) FBS). The cells were divided 24 h after infection into various dilutions (1:20 to 1:100), and selection was begun by adding medium containing 1.15 mg ml⁻¹ G418. New medium containing G418 was then introduced every 3 d. Visible antibiotic-resistant colonies were formed ~14 d after infection. These colonies were then picked and seeded onto new plates and propagated.

Immunofluorescence. Cells transfected with EYFP-clathrin-LCa were fixed in 2% (v/v) formaldehyde for 40 min. After washing with PBS, cells were permeabilized in PBS containing 10% (v/v) FBS, 3% (w/v) BSA and 0.5% (v/v) Triton X-100, and then incubated at 4 °C overnight with the monoclonal antibody against α-adaptin (Affinity Bioreagents), a subunit of the AP2 complex²⁵. The cells were then washed extensively with PBS containing 0.2% (w/v) BSA and 0.1% (v/v) Triton X-100 and incubated at room temperature for 30 min with FITC-conjugated goat anti-mouse IgG (Novus Biologicals). The FITC-conjugated antibodies were excited with a 488-nm argon ion laser (Melles Griot), and the fluorescence emission was collected using a filter that transmits 510–560-nm light. At the laser power used, the emission from EYFP in this detection wavelength range is negligible.

Fluorescence imaging. To obtain a simultaneous image of DiD-labeled viruses and EYFP-tagged clathrin, DiD was excited with a 633-nm helium-neon laser (Melles Griot), whereas EYFP was excited with a 532-nm diode-pumped Nd:YAG laser (CrystaLaser). A custom-designed polychroic beam splitter (Chroma) that reflects at wavelengths 520–550 nm and 615–655 nm was used to direct the laser lines onto the sample. The fluorescent emission from DiD and EYFP was collected by an oil-immersion objective with numerical aperture 1.45 (Olympus), spectrally separated by 610-nm long-pass dichroic mirrors (Chroma) and imaged onto two separate areas of the CCD camera (Roper Scientific, CoolSnap HQ). A 665-nm long-pass filter was used for DiD emission, and a bandpass filter that transmits 550–620-nm light was used for EYFP emission. Image series were recorded at 2 frames s⁻¹. For simultaneous imaging of DiD-labeled viruses and EGFP-tagged caveolin, a 488-nm argon ion laser (Melles Griot) was used to excite EGFP. A custom-designed polychroic beam splitter (Chroma) that reflects at 475–495 nm and 615–640 nm was used to direct the laser lines onto the sample. Differential interference contrast optics was used to obtain cell images before and after the fluorescence imaging. Experiments were conducted at 37 °C unless otherwise mentioned.

Image analysis. Each frame of the DiD fluorescence image series was processed by convolving with a Gaussian spatial filter to remove background and noise. Virus peaks were detected by recursively integrating over bright regions connected to each local maximum. The location of each virus was computed as the centroid of the bright region. Physical trajectories of viruses were reconstructed by pairing peaks in each frame to previously established trajectories according to proximity and similarity in intensity. The EYFP intensity associated with the virus was determined by subtracting a low-spatial frequency background signal in the EYFP channel and then integrating the EYFP signal weighted by the DiD signal of the virus. Only those viruses that started in the peripheral region of the cell surface and moved roughly within the focal plane were analyzed. Viruses that moved by a substantial amount orthogonally to the focal plane (out of focus) were not considered. Because BS-C-1 cells are comparatively flat, most virus trajectories remain close to the focal plane.

Note: Supplementary information is available on the Nature Structural & Molecular Biology website.

ACKNOWLEDGMENTS

We thank J.H. Keen (Thomas Jefferson University) and A. Helenius (Swiss Federal Institute of Technology) for their gifts of GFP-clathrin-LCa and Caveolin-1-EGFP plasmids, respectively. This work is supported in part by a Searle Scholarship, a Beckman Young Investigator award, the US Office of Naval Research and the US National Science Foundation (to X.Z.). M.J.R. is a US National Science Foundation pre-doctoral fellow.

COMPETING INTERESTS STATEMENT

The authors declare that they have no competing financial interests.

Received 2 December 2003; accepted 29 March 2004

Published online at <http://www.nature.com/nsmb/>

- Matlin, K.S., Reggio, H., Helenius, A. & Simons, K. Infectious entry pathway of influenza-virus in a canine kidney-cell line. *J. Cell Biol.* **91**, 601–613 (1981).
- Doxsey, S.J., Brodsky, F.M., Blank, G.S. & Helenius, A. Inhibition of endocytosis by anti-clathrin antibody. *Cell* **50**, 453–463 (1987).
- Anderson, H.A., Chen, Y.Z. & Norkin, L.C. Bound simian virus 40 translocates to caveolin-enriched membrane domains, and its entry is inhibited by drugs that selectively disrupt caveolae. *Mol. Biol. Cell* **7**, 1825–1834 (1996).
- Carbone, R. *et al.* Eps15 and eps15R are essential components of the endocytic pathway. *Cancer Res.* **57**, 5498–5504 (1997).
- Stang, E., Kartenbeck, J. & Parton, R.G. Major histocompatibility complex class I molecules mediate association of SV40 with caveolae. *Mol. Biol. Cell* **8**, 47–57 (1997).
- De Tulleo, L. & Kirchhausen, T. The clathrin endocytic pathway in viral infection. *EMBO J.* **17**, 4585–4593 (1998).
- Pelkmans, L., Kartenbeck, J. & Helenius, A. Caveolar endocytosis of simian virus 40 reveals a new two-step vesicular-transport pathway to the ER. *Nat. Cell Biol.* **3**, 473–483 (2001).
- Sieczkarski, S.B. & Whittaker, G.R. Influenza virus can enter and infect cells in the absence of clathrin-mediated endocytosis. *J. Virol.* **76**, 10455–10464 (2002).
- Pelkmans, L. & Helenius, A. Insider information: what viruses tell us about endocytosis. *Curr. Opin. Cell Biol.* **15**, 414–422 (2003).
- Nichols, B.J. & Lippincott-Schwartz, J. Endocytosis without clathrin coats. *Trends Cell Biol.* **11**, 406–412 (2001).
- Conner, S.D. & Schmid, S.L. Regulated portals of entry into cells. *Nature* **422**, 37–44 (2003).
- Brodsky, F.M., Chen, C.-Y., Knuehl, C., Towler, M.C. & Wakeham, D.E. Biological basket weaving: formation and function of clathrin-coated vesicles. *Annu. Rev. Cell Dev. Biol.* **17**, 517–568 (2001).
- Kirchhausen, T. Clathrin. *Annu. Rev. Biochem.* **69**, 699–727 (2000).
- Nabi, I.R. & Le, P.U. Caveolae/raft-dependent endocytosis. *J. Cell Biol.* **161**, 673–677 (2003).
- Scott, M.G.H., Benmerah, A., Muntaner, O. & Marullo, S. Recruitment of activated G protein-coupled receptors to pre-existing clathrin coated pits in living cells. *J. Biol. Chem.* **277**, 3552–3559 (2002).
- Santini, F., Gaidarov, I. & Keen, J.H. G protein-coupled receptor/arrestin3 modulation of the endocytic machinery. *J. Cell Biol.* **156**, 665–676 (2002).
- Gaidarov, I., Santini, F., Warren, R.A. & Keen, J.H. Spatial control of coated-pits dynamics in living cells. *Nat. Cell Biol.* **1**, 1–7 (1999).
- Skehel, J.J. & Wiley, D.C. Receptor binding and membrane fusion in viral entry: the influenza hemagglutinin. *Annu. Rev. Biochem.* **69**, 531–569 (2000).
- White, J., Helenius, A. & Gething, M.-J. Haemagglutinin of influenza virus expressed from a cloned gene promote membrane fusion. *Nature* **300**, 658–659 (1982).
- Yoshimura, A. & Ohnishi, S. Uncoating of influenza-virus in endosomes. *J. Virol.* **51**, 497–504 (1984).
- Martin, K. & Helenius, A. Transport of incoming influenza-virus nucleocapsids into the nucleus. *J. Virol.* **65**, 232–244 (1990).
- Lamb, R.A. & Krug, R.M. Orthomyxoviridae: the viruses and their replication. in *Fields Virology* (eds. Knipe, D.M. & Howley, P.M.) 1487–1531 (Lippincott Williams and Wilkins, Philadelphia, 2001).
- Klasse, P.J., Bron, R. & Marsh, M. Mechanisms of enveloped virus entry into animal cells. *Adv. Drug. Deliv. Rev.* **34**, 65–91 (1998).
- Helenius, A., Kartenbeck, J., Simons, K. & Fries, E. On the entry of Semliki Forest viruses into BHK-21 cells. *J. Cell Biol.* **84**, 404–420 (1980).
- Marrfield, C.J., Feldman, M.E., Wan, L. & Almers, W. Imaging actin and dynamin recruitment during invagination of single clathrin-coated pits. *Nat. Cell Biol.* **4**, 691–698 (2002).
- Volonte, D., Galbiati, F. & Lisanti, M.P. Visualization of caveolin-1, a caveolar marker protein, in living cells using green fluorescent protein (GFP) chimeras: the subcellular distribution of caveolin-1 is modulated by cell-cell contact. *FEBS Lett.* **445**, 431–439 (1999).
- Wu, X. *et al.* Clathrin exchange during clathrin-mediated endocytosis. *J. Cell Biol.* **155**, 291–300 (2001).
- Rappoport, J.Z. & Simon, S.M. Clathrin-mediated endocytosis during cell migration. *J. Cell Sci.* **116**, 847–855 (2003).
- Pelkmans, L., Punterer, D. & Helenius, A. Local actin polymerization and dynamin recruitment in SV-40-induced internalization of caveolae. *Science* **296**, 535–539 (2002).
- Thomsen, P., Roepstorff, K., Stahlhut, M. & Deurs, B.V. Caveolae are highly immobile plasma membrane microdomains, which are not involved in constitutive endocytic trafficking. *Mol. Biol. Cell* **13**, 238–250 (2002).
- Schnitzer, J.E., Oh, P., Pinney, E. & Allard, J. Filipin-sensitive caveolae-mediated transport in endothelium-reduced transcytosis, scavenger endocytosis, and capillary permeability of select macromolecules. *J. Cell Biol.* **127**, 1217–1232 (1994).
- Georgi, A., Mottola-Hartshorn, C., Warner, W., Fields, B. & Chen, L.B. Detection of individual fluorescently labelled reovirions in living cells. *Proc. Natl. Acad. Sci. USA* **87**, 6579–6583 (1990).
- Suomalainen, M. *et al.* Microtubule-dependent plus- and minus end-directed motilities are competing processes for nuclear targeting of adenovirus. *J. Cell Biol.* **144**, 657–672 (1999).
- Seisenberger, G. *et al.* Real-time single-molecule imaging of the infection pathway of an adeno-associated virus. *Science* **294**, 1929–1932 (2001).
- McDonald, D. *et al.* Visualization of the intracellular behavior of HIV in living cells. *J. Cell Biol.* **159**, 441–452 (2002).
- Lakadamyali, M., Rust, M.J., Babcock, H.P. & Zhuang, X. Visualizing infection of individual influenza viruses. *Proc. Natl. Acad. Sci. USA* **100**, 9280–9285 (2003).
- Wagner, R., Matrosovich, M. & Klenk, H.-D. Functional balance between haemagglutinin and neuraminidase in influenza virus infections. *Rev. Med. Virol.* **12**, 159–166 (2002).
- Babu, Y.S. *et al.* BCX-1812 (RWJ-270201): discovery of a novel, highly potent, orally active, and selective influenza neuraminidase inhibitor through structure-based drug design. *J. Med. Chem.* **43**, 3482–3486 (2000).
- Sidwell, R.W. *et al.* *In vivo* influenza virus-inhibitory effects of the cyclopentane neuraminidase inhibitor RWJ-270201. *Antimicrob. Agents Chemother.* **45**, 749–757 (2001).
- Rothenberg, K.G., Ying, Y.S., Kamen, B.A. & Anderson, R.G. Cholesterol controls the clustering of the glycoprophospholipid-anchored membrane-receptor for 5-methyltetrahydrofolate. *J. Cell Biol.* **111**, 2931–2938 (1990).
- Naslavsky, N., Weigert, R. & Donaldson, J.G. Convergence of non-clathrin-and clathrin-derived endosomes involves Arf6 inactivation and changes in phosphoinositides. *Mol. Biol. Cell* **14**, 417–431 (2003).
- Sieczkarski, S.B. & Whittaker, G.R. Differential requirements of Rab5 and Rab7 for endocytosis of influenza and other enveloped viruses. *Traffic* **4**, 333–343 (2003).
- Connolly, J.L., Green, S.A. & Greene, L.A. Pit formation and rapid changes in surface morphology of sympathetic neurons in response to nerve growth factors. *J. Cell Biol.* **90**, 176–180 (1981).
- Wilde, A. *et al.* EGF receptor signaling stimulates SRC kinase phosphorylation of clathrin, influencing clathrin redistribution and EGF uptake. *Cell* **96**, 677–687 (1999).
- Grimes, M.L. *et al.* Endocytosis of activated TrkA: evidence that nerve growth factor induces formation of signaling endosomes. *J. Neurosci.* **16**, 7950–7964 (1996).
- Beattie, E.C., Howe, C.L., Wilde, A., Brodsky, F.M. & Mobley, W.C. NGF signals through TrkA to increase clathrin at the plasma membrane and enhance clathrin-mediated membrane trafficking. *J. Neurosci.* **20**, 7325–7333 (2000).
- Peter, B.J. *et al.* BAR domains as sensors of membrane curvature: the amphiphysin BAR structure. *Science* **303**, 495–499 (2004).